CELL BIOLOGY

Broadly conserved roles of TMEM131 family proteins in intracellular collagen assembly and secretory cargo trafficking

Zhe Zhang[1], Meirong Bai[1], Guilherme Oliveira Barbosa[1], Andrew Chen[1], Yuehua Wei[1,2], Shuo Luo[1], Xin Wang[1], Bingying Wang[1], Tatsuya Tsukui[1,3], Hao Li[2], Dean Sheppard[1,3], Thomas B. Kornberg[1,2], Dengke K. Ma[1,4]*

Collagen is the most abundant protein in animals. Its dysregulation contributes to aging and many human disorders, including pathological tissue fibrosis in major organs. How premature collagen proteins in the endoplasmic reticulum (ER) assemble and route for secretion remains molecularly undefined. From an RNA interference screen, we identified an uncharacterized *Caenorhabditis elegans* gene *tmem-131*, deficiency of which impairs collagen production and activates ER stress response. We find that amino termini of human TMEM131 contain bacterial PapD chaperone–like domains, which recruit premature collagen monomers for proper assembly and secretion. Carboxy termini of TMEM131 interact with TRAPPC8, a component of the TRAPP tethering complex, to drive collagen cargo trafficking from ER to the Golgi. We provide evidence that previously undescribed roles of TMEM131 in collagen recruitment and secretion are evolutionarily conserved in *C. elegans*, *Drosophila*, and humans.

INTRODUCTION

Collagen is the major extracellular component of connective tissues and is the most abundant protein in animals (*1*–*3*). The production of mature collagen is a multistep process, involving collagen gene regulation, protein biosynthesis, posttranslational modifications in the endoplasmic reticulum (ER), formation of secretion-competent trimers, extracellular C-propeptide cleavage, and cross-linking among trimers (*1*–*3*). Dysregulation of collagen production or deposition contributes to a wide variety of human disorders, including diabetes, aging, and pathological tissue fibrosis in major organs such as kidneys, liver, lungs, and heart (*4*–*9*). The type I collagen is the most abundant fibril-type collagen; its trimer comprises two α1 (I) procollagen chains and one α2 (I) procollagen chain, encoded by the genes *COL1A1* and *COL1A2*, respectively. Both COL1A1 and COL1A2 contain C-terminal domains (C-propeptide) responsible for initial chain trimerization in the ER. The trimerization occurs via a zipper-like mechanism, initiating from the C-propeptide domain of α1/2 (I) in close proximity to ER membranes (*10*–*13*). Although the enzymes responsible for type I collagen modification, extracellular cleavage, and cross-linking have been well described (*1*, *14*), how procollagen monomers are recruited to assemble into secretion-competent multimers in the ER remains poorly understood.

COPII-coated vesicles mediate ER-to-Golgi anterograde transport of secretion-competent cargos, including those containing collagens (*15*, *16*). Tethering COPII vesicles from ER to Golgi membranes requires TRAPP (transport protein particle), a multisubunit protein complex highly conserved in eukaryotes (*17*–*19*). TRAPPC8 (trafficking protein particle complex 8) is a key component of TRAPP III, a subtype of TRAPP that acts as a guanine nucleotide exchange factor (GEF) to activate Rab GTPase (guanosine triphosphatase) to promote ER-to-Golgi cargo trafficking. Most COPII vesicles are approximately 60 to 80 nm in diameter, insufficient to accommodate 300- to 400-nm procollagen fibers (*15*). Collagen maturation and secretion in large-cargo COPII require HSP47, a procollagen chaperone in the ER, and TANGO1, an ER transmembrane protein that facilitates the export of specialized bulky cargo with collagen (*20*–*22*). HSP47 and TANGO1 orthologs are not apparently present in collagen-producing *Caenorhabditis elegans* (*23*–*25*), raising the question whether more broadly conserved mechanisms exist to facilitate procollagen assembly into export-competent collagen trimers en route for secretion.

In this study, we identify a previously uncharacterized *C. elegans* gene *tmem-131* that defines an evolutionarily conserved protein family important for procollagen recruitment and secretion. The exoskeleton cuticle of *C. elegans* is a complex collagen matrix that contains many distinct mature collagen proteins, including COL-19, an adult-specific, epithelial synthesized collagen (*26*). From yeast-two-hybrid (Y2H) screens, we identified two human proteins, COL1A2 and TRAPPC8, that bind to the N- and C-terminal domains of human TMEM131, respectively, and show that COL-19 secretion requires TMEM-131 and TRPP-8, the *C. elegans* ortholog of TRAPPC8. We show that TMEM131 proteins are also essential for collagen secretion in *Drosophila* and human cells, supporting the evolutionarily conserved role of TMEM131 protein family in collagen production.

RESULTS

Genome-wide RNAi screen identifies *tmem-131* regulating ER stress response and collagen production in *C. elegans*

We performed a genome-wide RNA interference (RNAi) screen for genes that affect levels of the *C. elegans* transgenic reporter *asp-17*p::GFP (Fig. 1A). *asp-17* is a gene encoding an aspartyl protease–like protein that is up-regulated by temperature stress and down-regulated by ER stress (Fig. 1, A to C) (*27*). From a screen of over 19,100 genes, we identified 574 RNAi clones that either up- or down-regulated the abundance of *asp-17*p::GFP (table S1). In this work, we

[1]Cardiovascular Research Institute, University of California, San Francisco, San Francisco, CA 94158, USA. [2]Department of Biochemistry and Biophysics, University of California, San Francisco, San Francisco, CA 94158, USA. [3]Department of Medicine, University of California, San Francisco, San Francisco, CA 94143, USA. [4]Department of Physiology, University of California, San Francisco, San Francisco, CA 94158, USA.
*Corresponding author. Email: dengke.ma@ucsf.edu

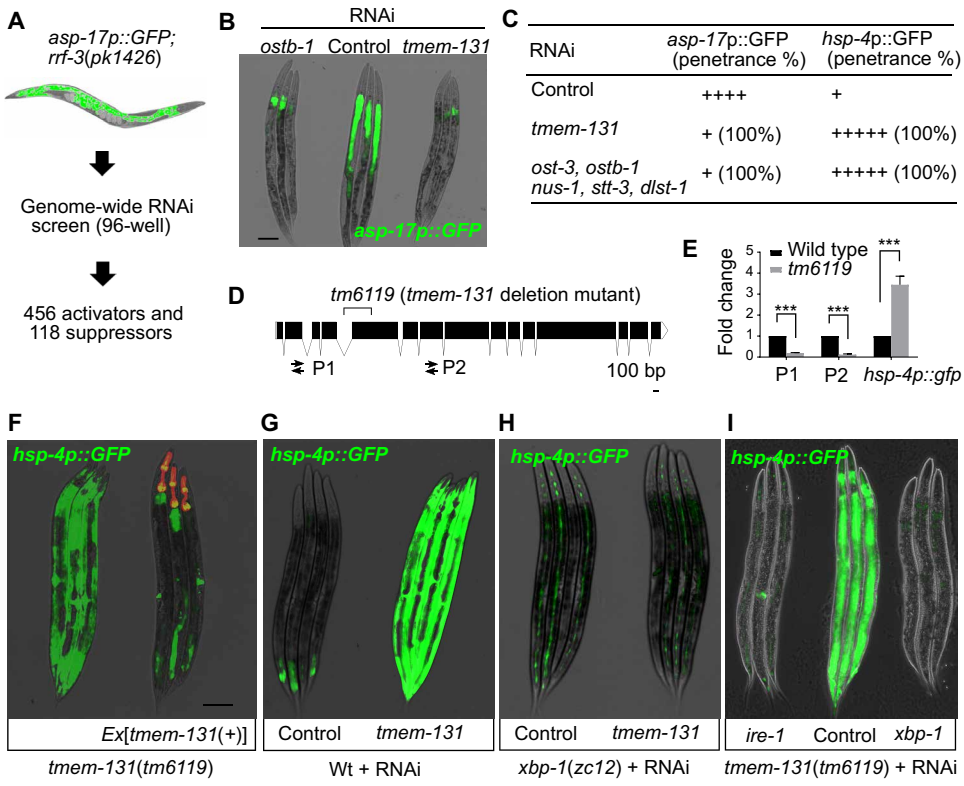

Fig. 1. Genome-wide RNAi screen identifies *tmem-131* regulating ER stress response in *C. elegans*. (**A**) Schematic of RNAi screen for regulators of *asp-17p*::GFP. For each 96-well plate, 10 L4-stage animals carrying *asp-17p*::GFP were placed in each well, triplicated for each gene RNAi treatment, and observed under stereoscopes when reaching adult stages. (**B**) Exemplar fluorescence and bright-field images for *rrf-3*; *asp-17p*::GFP with control, *ostb-1*, and *tmem-131* RNAi. (**C**) Table listing ER proteostasis genes whose RNAi also suppresses *rrf-3*; *asp-17p*::GFP ($n \geq 20$ for each group). (**D**) Schematic of Ce-*tmem-131* LOF alleles and RT-PCR P1 and P2 primers for *tmem-131* mRNA measurement. (**E**) Quantification of mRNA fold changes in *tmem-131* and *hsp-4::GFP* expression levels in wild-type and *tm6119* mutants. ***$P < 0.001$ ($n \geq 3$ biological replicates). (**F**) Exemplar fluorescence and bright-field images showing rescue of *hsp-4p*::GFP induction in *tmem-131*(*tm6119*) mutants with transgenic expression of *tmem-131*p::*tmem-131*::*gfp* marked by pharyngeal *myo-2*p::mCherry. (**G** to **I**) Exemplar fluorescence and bright-field images for the UPR reporter *hsp-4p*::GFP with *tmem-131* RNAi in wild-type (Wt) (G) and *xbp-1* mutants (H) and (I) in *tmem-131*(*tm6119*) mutants with control, *xbp-1*, or *ire-1* RNAi. Over 50 animals were observed, with three shown to indicate representative reporter expression. Scale bars, 100 μm.

focus on the gene *tmem-131*, as it is uncharacterized but otherwise highly evolutionarily conserved in all animals (see below). RNAi against *tmem-131* caused a fully penetrant and strong suppression of *asp-17*p::GFP reporter expression (Fig. 1B). By contrast, RNAi against *tmem-131* caused marked up-regulation of *hsp-4*p::GFP (Fig. 1C), an established transcriptional reporter for ER stress and unfolded protein response (UPR) in *C. elegans* (*28*–*30*). The screen also identified many other genes, including *ostb-1* and *dlst-1*, that are involved in protein modification and homeostasis in the ER (Fig. 1C). RNAi against *ostb-1* or *dlst-1*, as *tmem-131*, also caused marked up-regulation of *hsp-4*p::GFP and down-regulation of *asp-17*p::GFP (Fig. 1C).

To verify the RNAi phenotype, we examined *C. elegans* mutants carrying a 323–base pair (bp) genetic deletion allele *tm6119*, which caused a protein-coding frameshift and severe reduction of *tmem-131* expression level (Fig. 1, D and E). *tm6119* mutants exhibited abnormally elevated levels of *hsp-4*p::GFP that can be rescued by transgenic expression of green fluorescent protein (GFP)–tagged wild-type *tmem-131* (Fig. 1F). In addition, high *hsp-4*p::GFP levels in *tm6119* mutants or *tmem-131* RNAi–treated animals were completely suppressed by loss of function (LOF) of XBP-1 (Fig. 1, G to I), a transcription factor that drives a major branch of UPR in *C. elegans* (*29*–*32*). Loss of IRE-1, an ER transmembrane protein that senses ER stress, also prevented *hsp-4*p::GFP up-regulation in *tm6119* mutants (Fig. 1I). Besides constitutively activated *hsp-4*p::GFP expression, we found that TMEM131-deficient animals by RNAi or *tm6119* were smaller in size at higher temperature, more sensitive to the ER stressor tunicamycin as well as cuticle-disrupting osmotic stresses, and developed more slowly compared with wild type (fig. S1). Nonetheless, unlike *hsp-4*p::GFP, these additional phenotypes were not suppressed by loss of *xbp-1* or *ire-1* (fig. S1G). Together, these results indicate that loss of *tmem-131* causes various organismic phenotypes and defective ER homeostasis, leading to IRE-1– and XBP-1–dependent activation of *hsp-4*p::GFP and UPR.

To investigate the mechanism by which TMEM-131 may regulate ER function and proteostasis, we first examined its expression pattern and subcellular localization. The promoter of *tmem-131* drives expression of GFP in a variety of *C. elegans* tissues, most prominently the intestine and hypoderm (Fig. 2A). A translational reporter with GFP fused to the C terminus of TMEM-131 driven by the endogenous *tmem-131* promoter reveals an intracellular perinuclear reticulum pattern (Fig. 2B). The translational reporter rescued the *tm6119* mutant phenotype, indicating that the reticulum-localizing TMEM-131 is functional (Fig. 1F). In addition, SignalP-4.1 predicts an ER signal

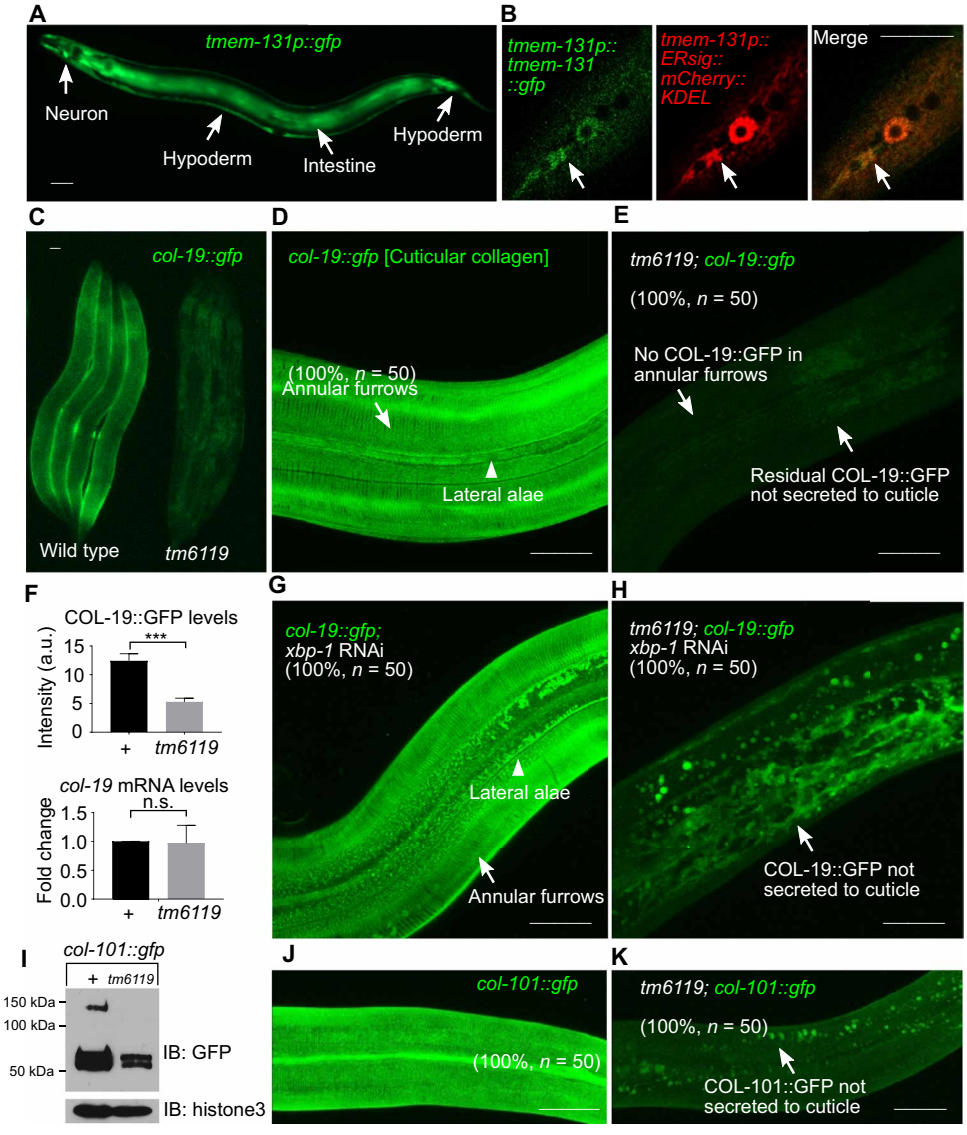

Fig. 2. Ce-TMEM131 is essential for secretion of GFP-labeled collagen COL-19 and COL-101. (**A**) Exemplar epifluorescence image of *tmem-131*p::GFP transcriptional reporter. Arrows indicate major tissues of reporter expression. (**B**) Exemplar confocal images of *tmem-131p::tmem-131*::GFP and ER transgenic reporter *tmem-131p::ERSig::mCherry::KDEL* showing colocalization (indicated by arrows) of both reporters with vesicular puncta patterns in the perinuclear areas of epithelial cells. (**C**) Exemplar epifluorescence image of *col-19*::GFP (i.e., *col-19*p::*col-19*::GFP) and *tm6119*; *col-19*::GFP. (**D** and **E**) Exemplar confocal fluorescence images with indicated phenotypic penetrance of *col-19*::GFP in wild-type (D) and *tmem-131* mutant (E). (**F**) Quantification of COL-19::GFP fluorescence intensity ($n \geq 4$ for each group) and endogenous *col-19* mRNA levels in wild-type and *tmem-131*(*tm6119*) mutants. a.u., arbitrary units. (**G** and **H**) Exemplar confocal fluorescence images with the indicated phenotypic penetrance of *col-19*::GFP with *xbp-1* RNAi in wild type (G) or *tmem-131* mutants (H). ***$P < 0.001$ ($n \geq 3$ biological replicates). n.s., no significant differences. (**I**) Exemplar SDS-PAGE and Western blot analysis of *col-101*::GFP and *tm6119*; *col-101*::GFP proteins from total animal lysates. IB, immunoblotting. (**J** and **K**) Exemplar confocal images with indicated phenotypic penetrance of *col-101*::GFP in wild-type (J) and *tmem-131* mutants (K). Scale bars, 20 μm.

peptide sequence (amino acids 1 to 30) of TMEM-131, supporting its ER endosomal localization (*33*). To confirm the prediction, we generated an mCherry-tagged ER reporter driven by the *tmem-131* promoter, with ER signal peptide at the N terminus and KDEL ER retention sequence at the C terminus. We found that TMEM131::GFP colocalized to the ER sig::mCherry::KDEL signal (Fig. 2B). Its cellular loci and regulation of *hsp-4*p::GFP led us to hypothesize that TMEM-131 normally acts to regulate processing, trafficking, and/or homeostasis of ER-resident proteins. To identify potential client proteins of TMEM-131, we screened a panel of translational fluorescent reporters for ER-resident transmembrane and secreted proteins, seeking any phenotypic defects caused by RNAi against *tmem-131* (table S2 and fig. S2). Among 34 various reporters we comprehensively examined, the COL-19::GFP reporter displayed the most notable defect in GFP patterns caused by *tmem-131* RNAi.

COL-19 is a *C. elegans* collagen protein that is secreted by the epithelial system and required for exoskeleton structure of the cuticle (*26*, *34*). COL-19::GFP deposition is enriched in the wild-type adult animal, constituting regular cuticle structures of annular furrows and lateral alae (Fig. 2, C and D). By contrast, cuticle COL-19::GFP is completely absent in the *tm6119* mutant, with apparently missing COL-19::GFP–marked annular furrows and weak intracellular

COL-19::GFP in the hypoderm (Fig. 2E). *tm6119* decreased the abundance of COL-19::GFP proteins without affecting the cuticle furrow structure (fig. S2F), the mRNA abundance, or the promoter activity of *col-19* (Fig. 2F and fig. S2G). The notable COL-19::GFP phenotype was not caused by UPR via activation of XBP-1, since *xbp-1* RNAi restored *hsp-4*p::GFP expression to normal levels (Fig. 1, G and H) but not epidermal COL-19::GFP in *tmem-131* mutants (Fig. 2, G and H). Knockdown of *xbp-1* by RNAi in the wild-type background caused excessive ER stresses but did not apparently affect COL-19::GFP in the cuticle (Fig. 2G). In the *tmem-131* mutant background, *xbp-1* RNAi caused more prominent intracellular accumulation of COL-19::GFP (Fig. 2H). By Western blot analysis, we found that *tm6119* decreased overall COL-19::GFP abundance irrespective of environmental temperature (fig. S2H), although the developmental or *hsp-4*p::GFP phenotype of *tm6119* mutants worsened at 25°C compared with 15° or 20°C (fig. S1). Among 34 various reporters we examined, mCherry-tagged EMB-9 (*35*), a collagen IV protein, was not affected by *tmem-131* RNAi (table S2). However, we found that two other cuticle collagen reporters, COL-101::GFP and LON-3::GFP, similarly required TMEM131 for normal collagen production (Fig. 2, I to K, and fig. S2F). *tm6119* decreased COL-101::GFP abundance most prominently in higher–molecular weight species (Fig. 2I). RNAi against *pdi-2*, which is essential for collagen folding and assembly (*36*), also partially decreased abundance of COL-19 (fig. S3, A and B). RNAi against *cup-2*, the Derlin ortholog essential for ER-associated degradation (ERAD) (*37*), caused synthetic lethality with *tm6119* (fig. S3, C and D), consistent with the observation that abnormally accumulated COL-19::GFP as ERAD substrate decreased in overall abundance in *tmem-131* mutants (Fig. 2). These results indicate that TMEM-131 is essential for mature collagen production, and its deficiency causes ER stress and UPR through abnormal accumulation of secreted proteins, including at least collagen COL-19, LON-3, and COL-101 in the ER.

Evolutionarily conserved roles of TMEM131 family proteins for collagen secretion

TMEM-131 has not been previously characterized, although it belongs to the highly evolutionarily conserved Pfam12371 (TMEM131_like) protein family (*38*–*40*). Its protein sequence is predicted by the program TOPCONS to contain two transmembrane segments, the first (i.e., signal peptide targeting to the ER) and second of which span a hydrophilic domain facing ER, endosomal lumen, or extracellular space, while the C-terminal part is predicted to localize in the cytosol (Fig. 3A) (*41*). We used structure homology modeling (SWISS-MODEL) (*42*) to search for proteins structurally similar to TMEM131 and identified many of those from bacteria that contain the PapD chaperone domain involved in the assembly and secretion of extracellular pilus components (fig. S4) (*43*, *44*). The PapD-like domain (PapD-L domain) in the N terminus of TMEM131 is predicted to be in the ER lumen (Fig. 3A), consistent with a putative role in procollagen processing. SWISS-MODEL also predicted a second PapD-L in the N terminus of TMEM131, albeit with lower similarity score. Structural comparisons further revealed that the *C. elegans* PapD-L, when modeled against one of the most similar structural homolog proteins from *Porphyromonas gingivalis* W83, comprises a two-loped immunoglobulin fold characteristic of canonic bacterial PapD domains (fig. S4, C and E) (*43*, *45*, *46*).

To determine the physiological importance of PapD-L of TMEM-131, we generated a precise deletion of the coding sequence for the PapD-L domain (amino acids 118 to 294) in *C. elegans tmem-131* (Ce-PapD) using CRISPR-Cas9 (Fig. 3B). Ce-PapD deletion recapitulated the *tmem-131(tm6119)* or *tmem-131* RNAi phenotype in strong *hsp-4*p::GFP induction and defective COL-19::GFP secretion, although quantitative reverse transcription polymerase chain reaction (qRT-PCR) results showed that Ce-PapD deletion did not affect the overall mRNA abundance of *tmem-131* (Fig. 3, C to F, and table S3). The phenotypes caused by *tm6119* were rescued by the wild-type (100%, $n = 20$), but not the PapD-lacking (0%, $n = 20$), transgenes of *tmem-131*. We further analyzed COL-19::GFP proteins by Western blot analysis after separation of soluble versus insoluble fractions, which contain monomeric procollagens and multimerized/cross-linked collagens, respectively, from whole animal lysates. Consistent with the notion that secreted COL-19::GFP is cross-linked, thus insoluble, we found that both *tm6119* and Ce-PapD deletion caused notable and robust decrease in the insoluble fractions of COL-19::GFP compared with wild type, while the abundance of soluble monomeric procollagens was less affected (Fig. 3G). These results indicate that Ce-PapD is essential for TMEM-131 to function in collagen recruitment and assembly, which is required for collagen secretion and preventing ER stress in *C. elegans*.

Within the evolutionarily conserved TMEM131_like protein family (Fig. 4A), the invertebrate model organisms *C. elegans* and *Drosophila* have one ortholog each, named *tmem-131* and *CG8370*, respectively. Vertebrate genomes encode two paralogs of TMEM-131, e.g., TMEM131 and KIAA0922 (also known as TMEM131L) in humans (Fig. 4, A and B). PapD-L domains are predicted from each homolog and represent the most highly conserved parts of TMEM131_like family proteins, based on multiple sequence alignment analysis (Clustal Omega) (fig. S4A). We sought to identify conserved protein-interacting partners as the ligand or client proteins for Ce-PapD in TMEM131 and used a Y2H screen to search for human proteins that can bind to Ce-PapD (Fig. 4C). From a normalized human complementary DNA (cDNA) library with approximately 9 million yeast clones in the screen, the Ce-PapD bait cDNA yielded 34 Ce-PapD interactor-encoding prey clones, among which COL1A2 was confirmed to interact with Ce-PapD in the Y2H assay (Fig. 4D and table S4). COL1A2 constitutes the type I collagen fibril together with COL1A1 (*2*, *47*). The library clone of human COL1A2 cDNA encodes the last 165 amino acid residues and a long 501 bp of the 3′ untranslated region (3′UTR) of full-length COL1A2. We recloned the C-propeptide domain of COL1A2 and confirmed its specific interaction with Ce-PapD (Fig. 4D). In addition to Ce-PapD, we found that the PapD-L domains from the *Drosophila* TMEM131 homolog CG8370 and human TMEM131, but not TMEM131L (also known as KIAA0922) (*39*), proteins can also interact with the C termini of human COL1A2 by Y2H assays (Fig. 4D). These results indicate that the TMEM131_like protein family members from *C. elegans*, *Drosophila*, and humans exhibit evolutionarily conserved biochemical interactions with the type I collagen protein COL1A2 via their PapD-L domains.

To test whether TMEM131_like proteins might have evolutionarily conserved functions in collagen secretion, we examined the loss-of-function phenotype of *CG8370* and *TMEM131* in *Drosophila* and human cells, respectively. In human cells, we used lentiviral expression of small-hairpin RNAs (shRNAs) to stably knock down *TMEM131* in the collagen-producing bone osteosarcoma U2OS cell line (Fig. 4, E and F, and fig. S5) (*48*). Immunofluorescence analysis revealed that *TMEM131* depletion markedly decreased secretion of extracelluar type I collagen fibers (green) (Fig. 4E), the severity of which is largely correlated

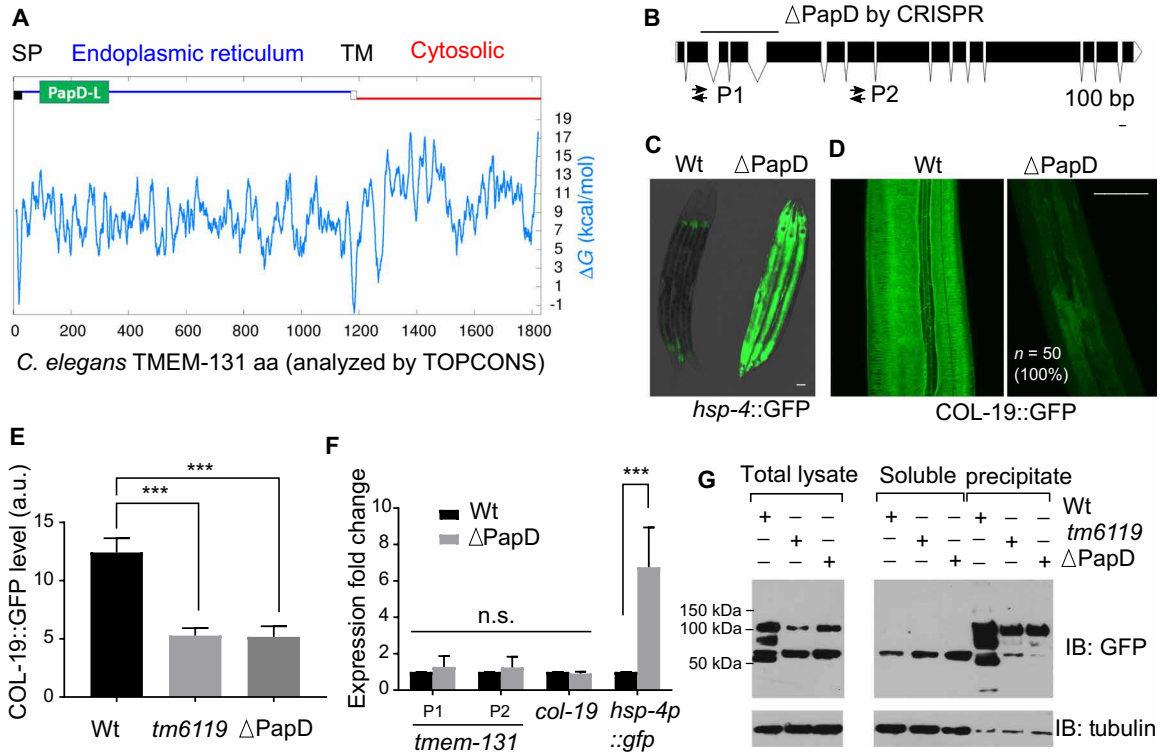

Fig. 3. PapD-L chaperone domains are essential for TMEM131 functions. (**A**) Schematic of *C. elegans* TMEM131 domain organization with PapD-L domain in green, ER localization in blue, and cytosol localization in red as predicted by the TOPCONS program (http://topcons.net/). The biological hydrophobicity scale calculates the free energy (Δ*G*) of membrane insertion for a window of 21 amino acids (aa) centered on each position in the TMEM131 sequence. (**B**) Schematic of *tmem-131* gene structure with the PapD-L deletion generated by CRISPR-Cas9 and RT-PCR P1 and P2 primers for *tmem-131* mRNA measurement. (**C** and **D**) Exemplar fluorescence images for *hsp-4p*::GFP (C) and *col-19*p::*col-19*::GFP with the indicated phenotypic penetrance (D) in wild-type and PapD-L deletion mutants. Scale bars, 20 μm. (**E**) Quantification of the COL-19::GFP fluorescence intensity in wild-type, *tmem-131*(*tm6119*), and *tmem-131*(ΔPapD-L) mutants. ***$P < 0.001$ ($n \geq 3$ biological replicates). (**F**) qRT-PCR measurements of endogenous *tmem-131*, *col-19*, and *hsp-4p*::*gfp* mRNA levels in wild-type and ΔPapD mutants. ***$P < 0.001$ ($n \geq 3$ biological replicates). (**G**) Exemplar Western blot analysis of COL-19::GFP in different fractions from wild-type, *tmem-131*(*tm6119*), and *tmem-131*(ΔPapD-L) mutants.

with the knockdown efficiency of shRNAs targeting five different coding sequences of *TMEM131* (Fig. 4, E and F, and fig. S5). Decreased type I collagen in TMEM131-depleted human cells is consistent with diminished COL-19::GFP abundance of *C. elegans tmem-131* mutants (Fig. 2). Fully penetrant synthetic lethality of LOFs for both *tmem-131* and the Derlin gene *cup-2* strongly indicates that the ERAD pathway degrades procollagens if not properly assembled and secreted (fig. S3D).

In *Drosophila*, we used the *Lsp2* > *Col4a1*:RFP transgenic fly to visualize fat body–secreted collagen and RNAi to silence expression of *CG8370* in fat body cells (*49*, *50*). We found that transgenic *CG8370* RNAi, but not control animals, accumulated collagen type IV alpha 1::RFP in fat body cells, indicative of defective collagen secretion (Fig. 5). In *Drosophila* fat body cells in which collagen is normally secreted to the hemolymph (insect blood), *tmem131* LOF caused collagen accumulation but did not appear to involve further degradation by ERAD. Nonetheless, these results collectively provide evidence that roles of TMEM131 proteins are evolutionarily conserved for collagen secretion in at least human and *Drosophila* cells.

TMEM131 promotes collagen cargo secretion through cytoplasmic C-terminal interaction with TRAPPC8

To address the mechanism by which the C-terminal domains of TMEM131 family proteins participate in collagen secretion, we used Y2H screens to identify proteins that can interact with the C terminus of human TMEM131 (Fig. 6A and table S5). Among the prey cDNA clones identified to confer interaction with human TMEM131 Ct (C-terminus) as the bait, we focused on TRAPPC8 in this study, as TRAPPC8-containing TRAPP III is critical for the ER-to-Golgi transport of collagen cargos. The TRAPPC8 prey clone identified encodes only part of its C-terminal region (Fig. 6, A and B). We subsequently verified interaction of the TRAPPC8 with TMEM131 Ct using coimmunoprecipitation assays (Fig. 6C). When coexpressed in human embryonic kidney (HEK) 293 cells, mCherry-tagged TMEM131 Ct specifically pulled down the GFP-tagged TRAPPC8 fragment. Using Y2H assays, we found that substitution of a highly conserved tripartite motif WRD to AAA in TRAPPC8 attenuated its interaction with TMEM131 Ct, whereas substitution of two highly conserved tryptophan residues to alanines in TMEM131 Ct attenuated its interaction with TRAPPC8 Ct, indicating that these residues are important for interaction and might constitute part of the interacting interface (Fig. 6D and fig. S6). Consistent with the interaction between TRAPPC8 and TMEM131, RNAi-mediated depletion of expression of *trpp-8*, the *C. elegans* homolog of *TRAPPC8*, strongly reduced the abundance of COL-19::GFP in the cuticle (Fig. 6E). RNAi against genes encoding additional components of TRAPP III also led to similar phenotype (table S6). Together, these results indicate that TMEM131 promotes collagen secretion not only

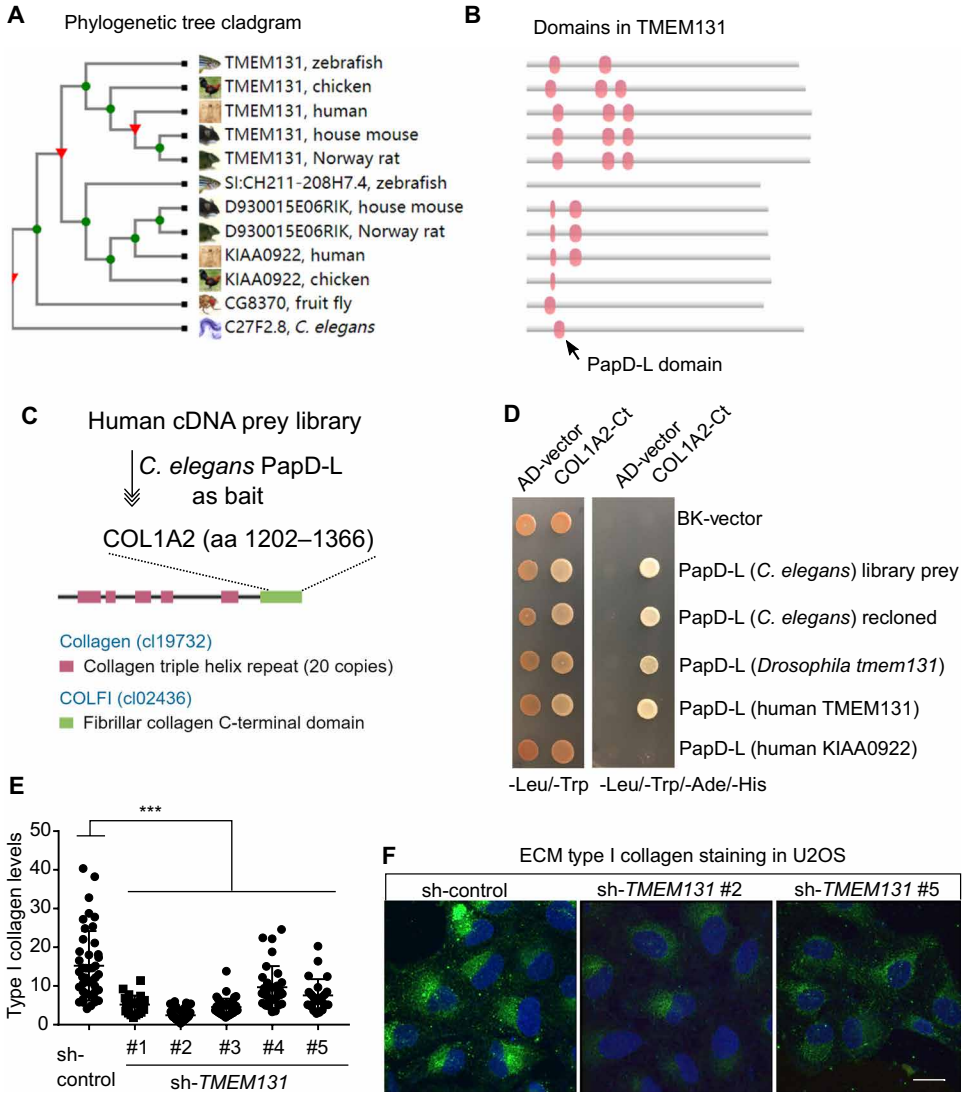

Fig. 4. Evolutionarily conserved role of TMEM131 for collagen secretion in human cells. (**A**) Cladogram of phylogenetic tree for the TMEM131 protein family from major metazoan species (adapted from www.wormbase.org). (**B**) Domain architectures of TMEM131 family proteins. (**C**) Schematic of Ce-PapD-L Y2H screens identifying the human COL1A2 C-terminal domain as an evolutionarily conserved binder of PapD-L. (**D**) Yeast colony growth in Y2H assays after retransformation of prey and bait vectors verifying the interaction between human COL1A2 C termini with PapD-L domains from *C. elegans*, *Drosophila*, and humans (photo credit: Zhe Zhang, UCSF). (**E**) Quantitative immunofluorescence measurements of extracellular collagen I fibers (green) in control and *TMEM131* shRNA–depleted cells; nuclei (blue). ***$P < 0.001$ ($N > 10$ cells for each condition; $n \geq 3$ biological replicates). (**F**) Exemplar confocal fluorescence images of U2OS cells with type I collagen staining after lentiviral expression of control shRNA and *TMEM131* shRNAs (#2 and #5). Scale bars, 20 μm.

by its N-terminal PapD-L domain but also by its C-terminal recruitment of TRAPP III for the ER-to-Golgi transport of collagen cargo.

Interaction of TMEM131 C terminus with TRAPPC8 prompted us to determine the in vivo consequence of deleting *tmem-131* C terminus on UPR and COL-19 in *C. elegans*. We used CRISPR-Cas9 to generate a precise deletion of the entire cytoplasmic domain (amino acids 1287 to 1808) of *tmem-131* and crossed the mutant to *hsp-4*p::GFP and COL-19::GFP reporters (table S3). We found that C-terminal deletion mutants showed strong dumpy phenotype, activation of *hsp-4*p::GFP, and reduction in COL-19::GFP abundance in cuticles (Fig. 7, A and B). To identify the specific subregion of TMEM131 Ct responsible for the interaction with TRAPPC8, we generated a series of TMEM131 Ct deletion mutants and test their interaction with TRAPPC8 in Y2H assays (Fig. 7C). Among the five deletions spanning the 1142– to 1883–amino acid sequence, only the very C-terminal end deletion (amino acids 1741 to 1883) abolished interaction with TRAPPC8 (Fig. 7D). We also generated five protein-coding mutations at evolutionarily conserved sites of TMEM131 Ct but found none of the single mutation can abolish the interaction with wild-type TRAPPC8 (Fig. 7E). By contrast, the C-terminal WRD->AAA mutation in TRAPPC8 attenuated interaction with wild-type TMEM131, indicating that the interaction interface between the two may require the WRD motif and multiple residues in TMEM131. Together, these results show that the C-terminal tail domain [TRAPID (TRAPP III–interacting domain)] of TMEM131 binds to TRAPPC8 (Fig. 7F), and its *C. elegans* counterpart is essential for collagen production in vivo.

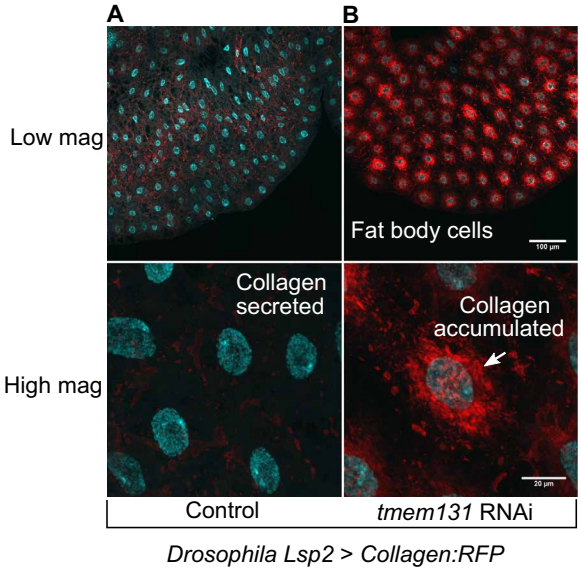

Fig. 5. Evolutionarily conserved role of TMEM131 for collagen secretion in *Drosophila*. (**A**) Exemplar confocal images of *Drosophila* fat body cells showing normal COL4A1 collagen secretion with control transgenic RNAi. (**B**) Exemplar confocal images of *Drosophila* fat body cells showing defective collagen secretion after fat body cell–specific transgenic RNAi of *Drosophila tmem131*. Both low-magnification (scale bar, 100 μm) and high-magnification (scale bar, 200 μm) views indicating collagen accumulation in fat body cells because of defective secretion of collagen to the hemolymph (insect blood) are shown.

DISCUSSION

In this work, we identify a *C. elegans* protein, TMEM-131, which has homologs in most animals, with essential roles in collagen secretion. These roles appear evolutionarily conserved for *Drosophila* and human TMEM131 homologs. We propose that TMEM131 proteins recruit premature collagen monomers through N-terminal PapD-L domains, whereas its C-terminal TRAPIDs bind to TRAPPC8, which promotes collagen secretion as a key component of TRAPP complex during the ER-to-Golgi transport of COPII vesicles (Fig. 7F). Although we did not recognize any apparent homologous C-propeptide protein sequence in *C. elegans* COL-19 or COL-101, their normal secretion still requires TMEM-131 as *Drosophila*, or human collagen I secretion requires TMEM131 homologs. Despite the lack of obvious sequence similarity between the *C. elegans* cuticle collagens and the COLFI domain of mammalian fibrillar collagens, TMEM131 family proteins appear to have evolved similar functions among different species. As COL-19::GFP secretion also requires *C. elegans* TRAPPC8 homolog, we propose that the interaction between the TMEM131 and TRAPPC8 family proteins and their essential roles in collagen secretion are evolutionarily conserved, while human TMEM131 evolved mechanisms to promote assembly of procollagens in the ER via direct binding of its PapD-L to procollagen. Together, these results have defined previously unknown physiological functions of conserved TMEM131 family proteins in collagen production and elucidated the underlying mechanism via TMEM131 interaction with PapD-L and TRAPPC8.

HSP47 is a collagen-specific chaperone that recognizes collagen trimers in the ER and prevents their premature aggregation during

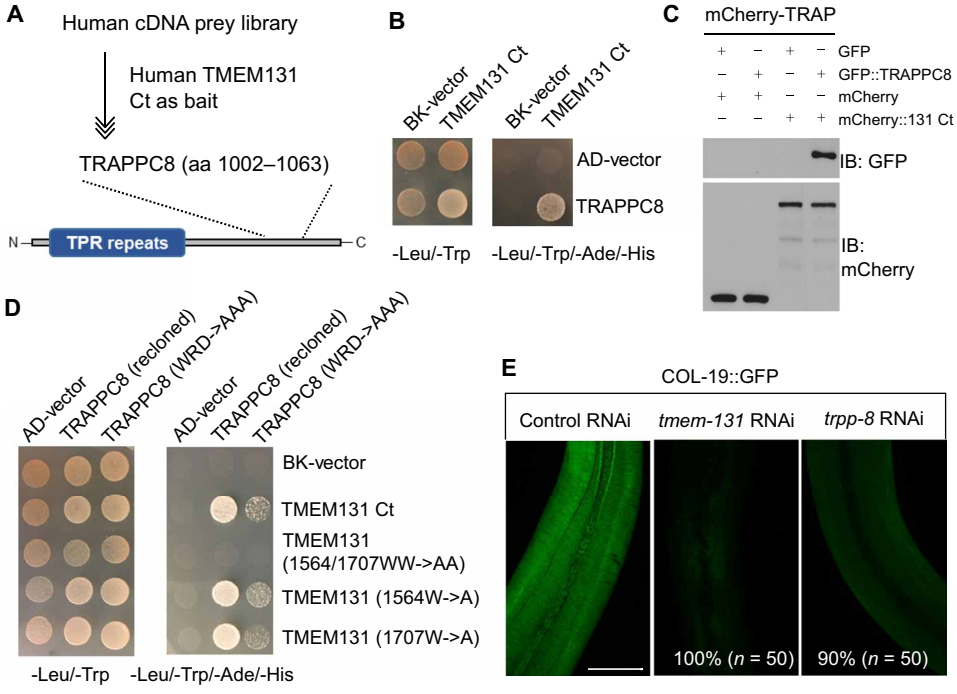

Fig. 6. Roles of TRAPPC8 in binding to TMEM131 and collagen secretion. (**A**) Schematic showing identification of TRAPPC8 as a TMEM131 interactor from Y2H screens. The C terminus of human TMEM131 as a bait yielded a prey cDNA clone encoding the amino acids 1002 to 1063 C-terminal region of TRAPPC8. (**B**) Yeast growth colonies verifying interaction of TMEM131 Ct and TRAPPC8 Ct (photo credit: Zhe Zhang, UCSF). (**C**) Coimmunoprecipitation and Western blot showing biochemical interaction of GFP-labeled TRAPPC8 fragment and mCherry-labeled TMEM131 Ct in human embryonic kidney (HEK) 293 cells. Cells were cotransfected with expression vectors, lysed for immunoprecipitation by mCherry-TRAP, and blotted by antibodies against GFP and mCherry. (**D**) Yeast growth colonies testing interaction of various TMEM131 Ct mutants with TRAPPC8 Ct or a mutant carrying WRD->AAA substitution, which attenuated interaction (photo credit: Zhe Zhang, UCSF). (**E**) Exemplar fluorescence images showing strongly decreased COL-19::GFP in *C. elegans* treated with RNAi against *tmem-131* or *trpp-8*. Scale bar, 50 μm.

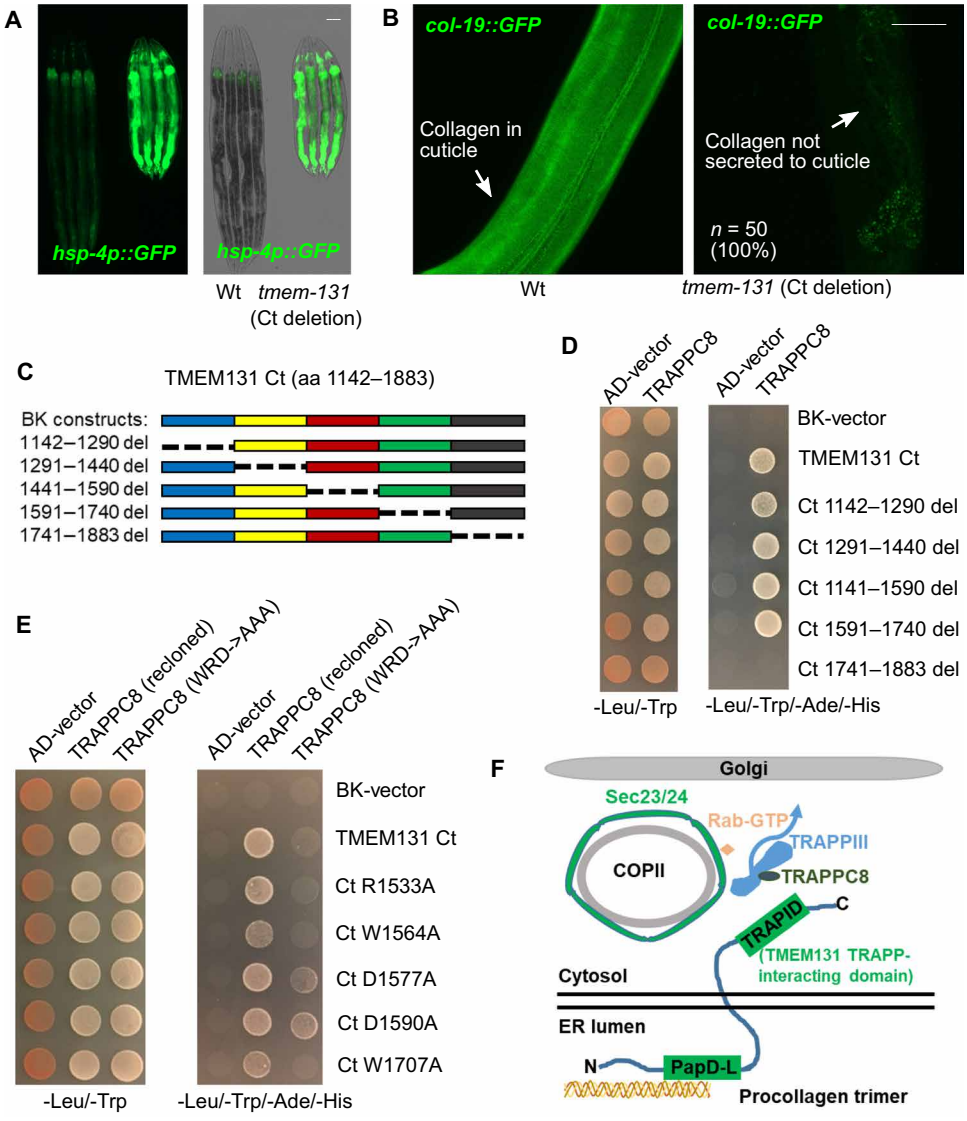

Fig. 7. TMEM131 promotes collagen secretion through cytoplasmic C-terminal interaction with TRAPPC8. (**A**) Exemplar fluorescence (left) and differential interference contrast merged (right) images showing activation of *hsp-4p::GFP* by CRISPR-mediated specific deletion of *C. elegans tmem-131* cytoplasmic C terminus. (**B**) Exemplar fluorescence images showing the abolished COL-19::GFP signal in the cuticle of mutants (right) with deletion of *tmem-131* cytoplasmic C terminus compared with wild type (left). Scale bar, 50 μm. (**C**) Schematic showing a series of deletions in human TMEM131 used for Y2H assays to identify regions responsible for binding to TRAPPC8. (**D**) Yeast colonies from Y2H assays showing interaction of TRAPPC8 with various TMEM131 Ct mutants (photo credit: Zhe Zhang, UCSF). (**E**) Yeast growth colonies from Y2H assays showing interaction of TRAPPC8 and a WRD->AAA mutant with TMEM131 Ct mutants with single alanine substitutions in the conserved C-terminal domain (photo credit: Zhe Zhang, UCSF). (**F**) Schematic model illustrating how TMEM131 regulates collagen secretion through its N-terminal PapD-L domain and C-terminal TRAPID. PapD-L binds to the C-propeptide domain of COL1A2 and facilitates assembly of procollagen trimers. TRAPID binds to TRAPPC8 and facilitates TRAPP III activation of Rab GTPase to promote the ER-to-Golgi transport of collagen cargo in COPII. For clarity, procollagen trimers in COPII and other essential factors for collagen secretion, including TANGO, HSP47, and SEC13/31, are not shown.

secretion (*51*). Collagen secretion also requires TANGO1, a protein that facilitates the assembly of a collagen export machine in the ER (*20*–*22*). However, no apparent HSP47 and TANGO1 orthologs can be found in *C. elegans* (*23*–*25*). Compared with HSP47 or TANGO1, TMEM131 family proteins are evolutionarily more ancient, consistent with their broad requirements for collagen production in animals. In mammals, COL1A1/2 trimerization initiates from the C-propeptide domain, which can be replaced with a transmembrane domain without affecting trimer formation (*10*). This indicates that C-propeptide domains act by bringing procollagens close to ER membranes to facilitate procollagen assembly and secretion. Supporting this notion, we obtained evidence for direct COL1A2 binding to the ER-luminal TMEM131 PapD-L domain and notable collagen production defects of TMEM131-deficient cells. Additional PapD-L interactors identified from Y2H screens suggest possibly broader roles of TMEM131 beyond COL1A2 binding, although TMEM131 does appear to exhibit client-protein specificity as many other secreted proteins, including the type IV collagen EMB-9, were not affected by LOF of *tmem-131* in

C. elegans (table S2). A recent CRISPR-based genetic screen identified both mammalian TMEM131 and TRAPCC8 that affect intracellular transport of several secreted proteins (*52*).

By Y2H assays, we found that TMEM131 PapD-L domains can interact with C-terminal propeptide domains of additional members of human collagen protein families (fig. S7). With a similar intriguing function in secretion, bacterial PapD acts as a chaperone that recruits and assembles pilus components for cellular export through well-defined "donor-strand exchange" (DSE) mechanisms (*44*, *53*, *54*). DSE proceeds through a concerted β strand displacement to orderly assemble pilus subunits before export to the bacterial periplasm. Whether PapD-L in TMEM131 acts by similar mechanisms for procollagens awaits further studies. Given our findings, we propose that TMEM131 family proteins play critical roles in recruiting procollagens on ER and/or secretory vesicular membranes to promote collagen assembly en route to secretion. As multicellular organisms evolved collagen-rich extracellular matrix, which is lacking in bacteria but analogous to bacterial pilus components, it is tempting to speculate that the role of PapD-L domains in collagen secretion originated from the homologous role of PapD in secretion of bacterial pilus components.

Our study also raises the intriguing possibility of TMEM131 as a new therapeutic target for alleviating tissue fibrosis in human disorders, treatment of which remains a major unmet medical need (*9*, *55*). Current antifibrotic strategies mostly leverage our knowledge on the well-characterized profibrotic mediators, including transforming growth factor–β (TGFβ), which stimulates collagen gene expression and protein biosynthesis. As TGFβ also controls gene expression involved in other biological processes than fibrosis, its inhibition can bring about many side effects, including epithelial hyperplasia, abnormal immune, and wound healing responses (*56*). Given the newly found role of TMEM131 in collagen secretion, inhibition of TMEM131 or its interfaces with collagen C–propeptide and TRAPPC8 may be therapeutically useful for treating pathological tissue fibrosis, including conditions in aging, systemic sclerosis, chronic inflammatory diseases, end-stage organ dysfunction, and heart failure (*6*, *9*, *57*, *58*). Realization of these therapeutic potentials will benefit from further studies on the mechanism of action, biological function, and regulation of TMEM131 family proteins in broad contexts of physiology and diseases.

MATERIALS AND METHODS

C. elegans culture and strains

C. elegans strains were grown on *Escherichia coli* at 20°C using standard methods, unless otherwise specified (*59*). Synchronized worm populations were obtained by bleaching gravid adults. Feeding RNAi-mediated knockdown was performed, as previously described (*60*, *61*).

The N2 Bristol strain was used as the wild type, and genotypes of strains used are as follows: *zcIs4* [*hsp-4*::GFP] V, *dmaIs8* [*hsp-16*p::GFP] IV, *rrf-3*(*pk1426*) II; *dmaIs10* [*asp-17*p::GFP, unc-54p::mCherry] X, *ire-1*(zc14) II; *zcIs4* V, *xbp-1*(*zc12*) III; *zcIs4* V, *kaIs12* [*col-19*::GFP], *dmaIs40* [*col-101*p::*col-101*::GFP (40 ng/μl); *unc-54*p::mCherry (40 ng/μl)], *kuIs55* [LON-3::GFP; *unc-119*(+)], and *tmem-131*(*tm6119*) III, which was further crossed with other reporters described above. Transgenic strains *dmaEx151* [*tmem-131*p::*tmem-131*::GFP (40 ng/μl); *myo-2*p::mCherry (40 ng/μl)], *dmaEx146* [*tmem-131*p::GFP (15 ng/μl); *unc-54*p::mCherry (10 ng/μl)], *dmaEx504* [*tmem-131*p::*tmem-131*::GFP (15 ng/μl); *tmem-131p*::ER signal::mCherry::KDEL (15 ng/μl);*myo-2*p::mCherry (10 ng/μl)], *dmaEx152* [*rpl-28p*::*F23H12.5*::mCherry (45 ng/μl); *unc-122*p::GFP (45 ng/μl)], *dmaEx153* [*rpl-28*p::*Y73E7A.8*::mCherry (45 ng/μl); *unc-122*p::GFP (45 ng/μl)], and *dmaEx169* [*rpl-28*p::*T19D2.1*::mCherry (45 ng/μl); *unc-122*p::GFP (45 ng/μl)] were generated by germline transformation, as described (*62*). The *tmem-131*(*dma301*) PapD-L deletion and *tmem-131*(*dma303*) C-terminal (amino acids 1287 to 1808) deletion strains were generated by CRISPR-Cas9 methods to induce double-stranded breaks and subsequent homologous repair (primer sequences are listed in table S3). Other translational reporters used to identify a phenotype affected by RNAi against *tmem-131* and cross with *tmem-131*(*tm6119*) include *arIs37* [*myo-3p::ssGFP + dpy-20*(+)], *bcIs39* [*lim-7p::ced-1::GFP+lin-15*(+)], *rme-4*(*b1001*); *bIs1* [*vit-2p::vit-2::GFP + rol-6*(+)], *caIs618* [*eff-1p::eff-1::gfp*], *cpg-1*(*tn1728*[*mng::3xflag::cpg-1*]) *III* , *dmaEx115* [*rpl-28p::manf-1::venus* 45ng/ μl], *dnSi4* [*gna-1p::GFP + Cbr-unc-119*(+)], *juEx1111* [*spon-1::vGFP*], *lrp-1*(*ku156*)*eqIs1* [*lrp-1p::lrp-1::GFP*]*I*; *rrf-3*(*pk1426*) *II*, *muIs49* [*egl-20::GFP+unc-22*(+)], *nIs590* [*fat-7p::fat-7cod::GFP*], *nuIs26* [*cat-1::GFP*], *pkIs2386* [*unc-54p::alpha synuclein::YFP*$^{+}$ *Cbr-unc-119*(+)] *IV*;*otIs181* [*dat-1::mCherry + ttx-3::mCherry*] *III*, *otEx1184* [*exl-1p::exl-1::GFP + rol-6*(+)], *osIs60* [*unc-54p::MIG-23::GFP; unc-119*(+)], *osIs64* [*myo-3p::YFP::TRAM;unc-119*(+)], *osIs66* [*myo-3p:: EGFP::WRK-1*], *osIs77* [*unc-54p::RFP::SP12; unc-119*(+)], *pwIs503* [*vha-6p::mans::GFP+ Cbr-unc-119*(+)], *qyIs44* [*emb-9p::EMB-9::mCherry*], *qyIs108* [*lam-1p::lam-1::dendra + unc-119*(+)], *rhIs23 III*[*GFP::him-4*], *sqIs11* [*lgg-1p::mCherry::GFP::lgg-1 + rol-6*(+)], *veIs13* [*col-19::GFP + rol-6*(+)] *V*; *let-7*(*mn112*) *unc-3*(*e151*) *X*; *mgEx725* [*lin-4::let-7 + ttx-3::RFP*], *vkEx1243* [*nhx-2p::ubiquitin-V::mCherry + myo-2p::GFP*], *vkEx1256 [nhx-2p::cpl-1::YFP + nhx-2p::dsRed::KDEL*], *vkEx1258* [*nhx-2p::cpl-1*(*W32AY35A*)*::YFP + nhx-2p::DsRed::KDEL*], *vkEx1260* [*nhx-2p::cpl-1::YFP + myo-2p::mCherry*], *vkEx1879* [*nhx-2p::cpl-1*(*W32A Y35A*)*::YFP + myo-2p::mCherry*], *xnIs96* [*hmr-1p::hmr-1::GFP*]. Extrachromosomal arrays were integrated using ultraviolet irradiation and backcrossed for three to six times.

Drosophila melanogaster experiments

Flies: UAS-Cg25C:RFP.2.1/CyO, Lsp2-Gal4/TM6B, and UAS-CG8370_dsRNA (Vienna Drosophila Resource Center ID no. 42509/GD). Lsp2-Gal4 expresses specifically in the fat body. Flies expressing collagen type IV alpha 1:RFP in fat body were crossed to either wild-type or UAS-CG8370_dsRNA flies. Fat body was dissected from wandering stage third instar larvae and fixed in 4% paraformaldehyde, stained with 4′,6-diamidino-2-phenylindole (DAPI), and mounted for imaging by confocal microscopy.

Quantitative reverse transcription polymerase chain reaction

Total RNA was extracted following the instructions of the Quick-RNA MiniPrep kit (Zymo Research, R1055) and reverse transcribed into cDNA (BioTools, B24408). Real-time PCR was performed by using SYBR Green Supermix (Thermo Fisher Scientific, FERK1081) on the Roche LightCycler96 (Roche, 05815916001) system. C_t values of specific genes were normalized to measurements of *act-1* (*C. elegans*) and *RPL13* (human cell lines) levels. Results are presented as fold changes to respective references. Statistical significance was determined with unpaired Student's *t* tests, one- or two-way analysis of variance (ANOVA) (comparisons across more than two groups), and adjusted with Bonferroni's corrections using GraphPad Prism 7. Primer sequences are listed in table S7.

Imaging and fluorescence quantification

SPE confocal (Leica) and digital automated epifluorescence microscopes (EVOS, Life Technologies) were used to capture fluorescence

images. Animals were randomly picked at the same stage and treated with 10 mM sodium azide and 1 mM levamisole in M9 solution (31742-250MG, Sigma-Aldrich), aligned on a 4% agar pad on a slide for imaging. Identical setting and conditions were used to compare experimental groups with control. For quantification of GFP fluorescence, animals were outlined and quantified by measuring gray values using the ImageJ software. The data were plotted and analyzed by using GraphPad Prism7.

Western blot analysis of proteins

Stage-synchronized animals for control and experiment groups were picked ($N > 40$) and lysed directly into 20 μl of Laemmli sample buffer for Western blot analysis. Proteins were resolved by 15% SDS–polyacrylamide gel electrophoresis (PAGE) (Bio-Rad, 4561084) and transferred to a nitrocellulose membrane (Bio-Rad, 1620167). Proteins of interest were detected using antibodies against GFP (A02020, Abbkine), tubulin (Sigma-Aldrich, T5168), and H3 (Abcam, ab1791). All experiments were repeated for multiple times.

For subcellular fractionation, 50-ml adult-stage animal pellets were washed with M9 buffer three times and resuspended in 500 μl of RIPA lysis buffer (Amresco, N653) with 10 mM phenylmethylsulfonyl fluoride (PMSF) and protease inhibitor cocktail (BioTools, B14002). Then, pellet samples were disrupted by TissueRuptor (motor unit "8" for 1 min) and incubated for 45 min in a 4°C cold room. The lysate was centrifuged at 13,000 rpm for 15 min, the supernatant was collected as the soluble part, and the pellet was resuspended in 500 μl of RIPA lysis buffer with 10 mM PMSF and protease inhibitor cocktail as the insoluble part. Samples (20 μl) added with equal volume of 2× Laemmli sample buffer were subject to Western blot analysis, as described above.

Y2H assay

The cDNA coding sequences of the PapD-L domain of *C. elegans* TMEM131 and the C-terminal TRAPID of human TMEM131 were cloned into the pGBKT7 vector and screened with a normalized universal human cDNA library (Clontech, 630481), following instructions in the Matchmaker Gold Yeast Two-Hybrid System (Clontech, 630489). Verification of positive colonies was achieved by cotransforming PapD-L domains from different species (in pGBKT7 vector) and genes of interest (in pGADT7 vector) following the instruction of the Yeastmaker Yeast Transformation System 2 (Clontech, 630439), as well as plasmids from recloned cDNA.

Genome-wide RNAi screen in *C. elegans*

Genome-wide RNAi screen in *C. elegans* was carried out by using the Ahringer library in a 96-well plate format modified from published protocol (*60*, *61*). Briefly, double-stranded RNA (dsRNA)–expressing bacteria were replicated from Ahringer library to black-well, clear, and flat-bottom 96-well plate containing 100 μl of LB medium with carbenicillin (100 μg/ml) and cultured overnight at 37°C without shaking. One hundred microliters of LB containing isopropyl-β-D-thiogalactopyranoside (IPTG) (2 to 4 μg/ml) was added into each well to induce dsRNA expression for 2 hours. Bacteria containing dsRNA were then collected by centrifugation and resuspended in 50 μl of nematode growth medium containing carbenicillin (50 μg/ml), IPTG (1 μg/ml), and ~10 synchronized L1 worms. The animals were cultured at 25°C with shaking at the speed of 150 rpm for 3 days. Microscopic examination was then carried out looking for aberrant GFP reporter expression and other phenotypes.

Synthetic lethality analysis in *C. elegans*

Wild-type and *tmem-131(tm6119)* mutants were grown on *E. coli* at 20°C using standard methods for several (>2) generations. Two L3–L4 stage worms were picked into the RNAi plate for testing with the methods mentioned for synthetic genetic-interaction analysis, as described (*63*). *spg-7* (RNAi) was a positive control for RNAi efficiency. Over the course of 5 days, the number of progenies at adult stage was counted. The growth score was assigned from 0 to 6 (0: 2 parental worms; 1: 1 to 10 progeny; 2: 11 to 50 progeny; 3: 51 to 100 progeny; 4: 101 to 150 progeny; 5: 151 to 200 progeny; and 6: 200+ progeny), with at least three biological replicates.

Lentiviral TMEM131 shRNA knockdown in cultured human U2OS cells

Human TMEM131 knockdown in osteosarcoma U2OS cells was carried out with lentiviral shRNA (Sigma-Aldrich, SHCLNG-NM_015348). The TMEM131 shRNA targeting sequences are as follows: 5′-TAGCAGTTTCTCACCTATAAT-3′ [TRCN0000257459, CDS (coding sequence)], 5′-ATTATGCGCCAAGATCTAATT-3′ (TRCN0000246000, 3′UTR), 5′-TCCAATTGAGTTGGCTATAAA-3′ (TRCN0000246001, CDS), 5′-CTCGGACCCTTGGTCTAATTC-3′ (TRCN0000246002, CDS), 5′-CATAGATTGAGTGCTATATTT-3′ (TRCN0000246003, CDS). HEK293T was transfected by the pMD2.G, psPAX2, and shRNA plasmids, following the lentivirus production methods and manuals of TurboFect Transfection Reagent (Thermo Fisher Scientific, R0531). The lentivirus-based GFP-specific shRNAs were used as negative controls (Addgene, 31849). Forty-eight hours later, the TMEM131 shRNA lentivirus–containing media were collected and filtrated by a 0.45-μm syringe filter (Millipore EMD, SLHP033RS). The osteosarcoma U2OS cells were incubated with TMEM131 shRNA lentivirus medium for 24 hours in a humidified incubator at 37°C with 5% CO_2. Transduction efficacy was enhanced by adding Polybrene (Sigma-Aldrich, TR-1003-G). Lentivirus-transduced cells were enriched by the medium with puromycin selection (1.5 μg/ml) for 3 days. Ascorbates were exogenously supplemented to ensure proper collagen modification. The knockdown efficiency of TMEM131 shRNA was evaluated by qRT-PCR.

Immunofluorescence staining of type I procollagen in human U2OS cells

The human TMEM131 knockdown U2OS stable cells were seeded in 24-well plates with cover glass for 2 days, each with three replicates (Fisher Scientific, 22293232). After 1× phosphate-buffered saline (PBS) washing for once, cells were treated by 4% formaldehyde solution for 10 min. With 1× PBS washing for three times, cells were treated with 0.2% Triton X-100 in 1× PBS solution for 15 min. Then, cells were incubated in 5% bovine serum albumin in 1× PBS solution for 1 hour at 4°C after 1× PBS washing for three times. Monoclonal anti-human Procollagen Type I C-Peptide (PIP) clone PC5-5 (Takara Bio USA, M011) was incubated with the cell sample at 4°C for 12 hours then with goat anti-mouse IgG (H+L) Alexa Fluor 488 oligoclonal secondary antibody for 1 hour (Fisher Scientific, A-11001). Following 1× PBS washing for three times, the cover slide with cell samples was sealed on the microscope slide with Fluoroshield Mounting Medium with DAPI (Thermo Fisher Scientific, NC0200574). For quantification of GFP fluorescence, every cell in the captured images was outlined and quantified by measuring gray values of fluorescence intensity using the ImageJ software. The data were plotted and analyzed by using GraphPad Prism7.

SUPPLEMENTARY MATERIALS

Supplementary material for this article is available at http://advances.sciencemag.org/cgi/content/full/6/7/eaay7667/DC1

Fig. S1. Additional phenotypic characterization of *tmem-131*(*tm6119*) mutants.
Fig. S2. Fluorescent reporter screens and mutant verification for *tmem-131* phenotype.
Fig. S3. Genetic interaction of *tmem-131* with other genes involved in collagen production and degradation.
Fig. S4. Sequence and structural similarities of Ce-PapD-L and other known PapD domain–containing proteins.
Fig. S5. Verification of human *TMEM131* shRNA knockdown efficiency.
Fig. S6. Conserved residues in TRAPPC8 and TMEM131 C termini.
Fig. S7. Y2H assay of interaction between PapD-L from TMEM131 and collagen family proteins with C-terminal COLFI domains.
Table S1. List of genes identified from genome-wide RNAi screen of *asp-17*p::GFP regulators.
Table S2. Reporters examined in phenotypic screens for *tmem-131* RNAi.
Table S3. Primers and oligos used in genomic editing.
Table S4. List of human cDNA clones identified by Y2H screens using Ce-PapD-L as a bait.
Table S5. List of human cDNA clones identified by Y2H screens using TMEM131 Ct as a bait.
Table S6. Genes required for COL-19::GFP production in *C. elegans* based on RNAi.
Table S7. qRT-PCR primers used in this study.

View/request a protocol for this paper from *Bio-protocol*.

REFERENCES AND NOTES

1. J. Myllyharju, K. I. Kivirikko, Collagens, modifying enzymes and their mutations in humans, flies and worms. *Trends Genet.* **20**, 33–43 (2004).
2. M. D. Shoulders, R. T. Raines, Collagen structure and stability. *Annu. Rev. Biochem.* **78**, 929–958 (2009).
3. M. J. Mienaltowski, D. E. Birk, Structure, physiology, and biochemistry of collagens. *Adv. Exp. Med. Biol.* **802**, 5–29 (2014).
4. R. Bataller, D. A. Brenner, Liver fibrosis. *J. Clin. Invest.* **115**, 209–218 (2005).
5. B. D. Humphreys, Mechanisms of renal fibrosis. *Annu. Rev. Physiol.* **80**, 309–326 (2018).
6. W. McKleroy, T.-H. Lee, K. Atabai, Always cleave up your mess: Targeting collagen degradation to treat tissue fibrosis. *Am. J. Phys. Lung Cell. Mol. Phys.* **304**, L709–L721 (2013).
7. K. C. Meyer, Pulmonary fibrosis, part I: Epidemiology, pathogenesis, and diagnosis. *Expert Rev. Respir. Med.* **11**, 343–359 (2017).
8. L. A. Murtha, M. J. Schuliga, N. S. Mabotuwana, S. A. Hardy, D. W. Waters, J. K. Burgess, D. A. Knight, A. J. Boyle, The processes and mechanisms of cardiac and pulmonary fibrosis. *Front. Physiol.* **8**, 777 (2017).
9. T. A. Wynn, T. R. Ramalingam, Mechanisms of fibrosis: Therapeutic translation for fibrotic disease. *Nat. Med.* **18**, 1028–1040 (2012).
10. N. J. Bulleid, J. A. Dalley, J. F. Lees, The C-propeptide domain of procollagen can be replaced with a transmembrane domain without affecting trimer formation or collagen triple helix folding during biosynthesis. *EMBO J.* **16**, 6694–6701 (1997).
11. J. F. Lees, M. Tasab, N. J. Bulleid, Identification of the molecular recognition sequence which determines the type-specific assembly of procollagen. *EMBO J.* **16**, 908–916 (1997).
12. J. Engel, D. J. Prockop, The zipper-like folding of collagen triple helices and the effects of mutations that disrupt the zipper. *Annu. Rev. Biophys. Biophys. Chem.* **20**, 137–152 (1991).
13. U. Sharma, L. Carrique, S. Vadon-Le Goff, N. Mariano, R.-N. Georges, F. Delolme, P. Koivunen, J. Myllyharju, C. Moali, N. Aghajari, D. J. S. Hulmes, Structural basis of homo- and heterotrimerization of collagen I. *Nat. Commun.* **8**, 14671 (2017).
14. R. A. F. Gjaltema, R. A. Bank, Molecular insights into prolyl and lysyl hydroxylation of fibrillar collagens in health and disease. *Crit. Rev. Biochem. Mol. Biol.* **52**, 74–95 (2017).
15. V. Malhotra, P. Erlmann, The pathway of collagen secretion. *Annu. Rev. Cell Dev. Biol.* **31**, 109–124 (2015).
16. G. Zanetti, K. B. Pahuja, S. Studer, S. Shim, R. Schekman, COPII and the regulation of protein sorting in mammals. *Nat. Cell Biol.* **14**, 20–28 (2011).
17. J. Barrowman, D. Bhandari, K. Reinisch, S. Ferro-Novick, TRAPP complexes in membrane traffic: Convergence through a common Rab. *Nat. Rev. Mol. Cell Biol.* **11**, 759–763 (2010).
18. J. J. Kim, Z. Lipatova, N. Segev, TRAPP Complexes in Secretion and Autophagy. *Front. Cell Dev. Biol.* **4**, 20 (2016).
19. S. Zhao, C. M. Li, X. M. Luo, G. K. Y. Siu, W. J. Gan, L. Zhang, W. K. K. Wu, H. C. Chan, S. Yu, Mammalian TRAPPIII Complex positively modulates the recruitment of Sec13/31 onto COPII vesicles. *Sci. Rep.* **7**, 43207 (2017).
20. I. Raote, M. Ortega-Bellido, A. J. Santos, O. Foresti, C. Zhang, M. F. Garcia-Parajo, F. Campelo, V. Malhotra, TANGO1 builds a machine for collagen export by recruiting and spatially organizing COPII, tethers and membranes. *eLife* **7**, e32723 (2018).
21. R. Venditti, T. Scanu, M. Santoro, G. Di Tullio, A. Spaar, R. Gaibisso, G. V. Beznoussenko, A. A. Mironov, A. Mironov, L. Zelante, M. R. Piemontese, A. Notarangelo, V. Malhotra, B. M. Vertel, C. Wilson, M. A. De Matteis, Sedlin controls the ER export of procollagen by regulating the Sar1 cycle. *Science* **337**, 1668–1672 (2012).
22. K. Saito, M. Chen, F. Bard, S. Chen, H. Zhou, D. Woodley, R. Polischuk, R. Schekman, V. Malhotra, TANGO1 facilitates cargo loading at endoplasmic reticulum exit sites. *Cell* **136**, 891–902 (2009).
23. J. Huxley-Jones, D. L. Robertson, R. P. Boot-Handford, On the origins of the extracellular matrix in vertebrates. *Matrix Biol.* **26**, 2–11 (2007).
24. M. G. Hanna, J. L. Peotter, E. B. Frankel, A. Audhya, Membrane transport at an organelle interface in the early secretory pathway: Take your coat off and stay a while: Evolution of the metazoan early secretory pathway. *BioEssays* **2018**, e1800004 (2018).
25. A. Chioran, S. Duncan, A. Catalano, T. J. Brown, M. J. Ringuette, Collagen IV trafficking: The inside-out and beyond story. *Dev. Biol.* **431**, 124–133 (2017).
26. M. C. Thein, G. McCormack, A. D. Winter, I. L. Johnstone, C. B. Shoemaker, A. P. Page, *Caenorhabditis elegans* exoskeleton collagen COL-19: An adult-specific marker for collagen modification and assembly, and the analysis of organismal morphology. *Dev. Dyn.* **226**, 523–539 (2003).
27. W. Jiang, Y. Wei, Y. Long, A. Owen, B. Wang, X. Wu, S. Luo, Y. Dang, D. K. Ma, A genetic program mediates cold-warming response and promotes stress-induced phenoptosis in *C. elegans*. *eLife* **7**, e35037 (2018).
28. V. Kapulkin, B. G. Hiester, C. D. Link, Compensatory regulation among ER chaperones in C. elegans. *FEBS Lett.* **579**, 3063–3068 (2005).
29. M. Calfon, H. Zeng, F. Urano, J. H. Till, S. R. Hubbard, H. P. Harding, S. G. Clark, D. Ron, IRE1 couples endoplasmic reticulum load to secretory capacity by processing the XBP-1 mRNA. *Nature* **415**, 92–96 (2002).
30. R. C. Taylor, A. Dillin, XBP-1 is a cell-nonautonomous regulator of stress resistance and longevity. *Cell* **153**, 1435–1447 (2013).
31. J. Sun, Y. Liu, A. Aballay, Organismal regulation of XBP-1-mediated unfolded protein response during development and immune activation. *EMBO Rep.* **13**, 855–860 (2012).
32. C. E. Richardson, S. Kinkel, D. H. Kim, Physiological IRE-1-XBP-1 and PEK-1 signaling in *Caenorhabditis elegans* larval development and immunity. *PLOS Genet.* **7**, e1002391 (2011).
33. T. N. Petersen, S. Brunak, G. von Heijne, H. Nielsen, SignalP 4.0: Discriminating signal peptides from transmembrane regions. *Nat. Methods* **8**, 785–786 (2011).
34. I. L. Johnstone, The cuticle of the nematode *Caenorhabditis elegans*: A complex collagen structure. *BioEssays* **16**, 171–178 (1994).
35. S. Ihara, E. J. Hagedorn, M. A. Morrissey, Q. Chi, F. Motegi, J. M. Kramer, D. R. Sherwood, Basement membrane sliding and targeted adhesion remodels tissue boundaries during uterine-vulval attachment in *Caenorhabditis elegans*. *Nat. Cell Biol.* **13**, 641–651 (2011).
36. A. D. Winter, G. McCormack, A. P. Page, Protein disulfide isomerase activity is essential for viability and extracellular matrix formation in the nematode *Caenorhabditis elegans*. *Dev. Biol.* **308**, 449–461 (2007).
37. H. Dang, T. I. Klokk, B. Schaheen, B. M. McLaughlin, A. J. Thomas, T. A. Durns, B. G. Bitler, K. Sandvig, H. Fares, Derlin-dependent retrograde transport from endosomes to the golgi apparatus. *Traffic* **12**, 1417–1431 (2011).
38. J. Ruan, H. Li, Z. Chen, A. Coghlan, L. J. M. Coin, Y. Guo, J.-K. Hériché, Y. Hu, K. Kristiansen, R. Li, T. Liu, A. Moses, J. Qin, S. Vang, A. J. Vilella, A. Ureta-Vidal, L. Bolund, J. Wang, R. Durbin, TreeFam: 2008 Update. *Nucleic Acids Res.* **36**, D735–D740 (2008).
39. N. Maharzi, V. Parietti, E. Nelson, S. Denti, M. Robledo-Sarmiento, N. Setterblad, A. Parcelier, M. Pla, F. Sigaux, J. C. Gluckman, B. Canque, Identification of TMEM131L as a novel regulator of thymocyte proliferation in humans. *J. Immunol.* **190**, 6187–6197 (2013).
40. S. Szuplewski, N. Maharzi, E. Nelson, K. Alhaj Hussen, B. Mignotte, I. Guénal, B. Canque, Evolutionary conservation of Notch signaling inhibition by TMEM131L overexpression. *Biochem. Biophys. Res. Commun.* **486**, 909–915 (2017).
41. K. D. Tsirigos, C. Peters, N. Shu, L. Käll, A. Elofsson, The TOPCONS web server for consensus prediction of membrane protein topology and signal peptides. *Nucleic Acids Res.* **43**, W401–W407 (2015).
42. A. Waterhouse, M. Bertoni, S. Bienert, G. Studer, G. Tauriello, R. Gumienny, F. T. Heer, T. A. P. de Beer, C. Rempfer, L. Bordoli, R. Lepore, T. Schwede, SWISS-MODEL: Homology modelling of protein structures and complexes. *Nucleic Acids Res.* **46**, W296–W303 (2018).
43. A. Holmgren, C.-L. Bränden, Crystal structure of chaperone protein PapD reveals an immunoglobulin fold. *Nature* **342**, 248–251 (1989).
44. F. G. Sauer, K. Fütterer, J. S. Pinkner, K. W. Dodson, S. J. Hultgren, G. Waksman, Structural basis of chaperone function and pilus biogenesis. *Science* **285**, 1058–1061 (1999).
45. B. Ford, D. Verger, K. Dodson, E. Volkan, M. Kostakioti, J. Elam, J. Pinkner, G. Waksman, S. Hultgren, The structure of the PapD-PapGII pilin complex reveals an open and flexible P5 pocket. *J. Bacteriol.* **194**, 6390–6397 (2012).
46. M. J. Kuehn, D. J. Ogg, J. Kihlberg, L. N. Slonim, K. Flemmer, T. Bergfors, S. J. Hultgren, Structural basis of pilus subunit recognition by the PapD chaperone. *Science* **262**, 1234–1241 (1993).
47. H. Lodish, A. Berk, S. L. Zipursky, P. Matsudaira, D. Baltimore, J. Darnell, Collagen: The fibrous proteins of the matrix. Molecular Cell Biology, 4th Ed. (2000); www.ncbi.nlm.nih.gov/books/NBK21582/.

48. C. Pautke, M. Schieker, T. Tischer, A. Kolk, P. Neth, W. Mutschler, S. Milz, Characterization of osteosarcoma cell lines MG-63, Saos-2 and U-2 OS in comparison to human osteoblasts. *Anticancer Res.* **24**, 3743–3748 (2004).
49. J. C. Pastor-Pareja, T. Xu, Shaping cells and organs in Drosophila by opposing roles of fat body-secreted Collagen IV and perlecan. *Dev. Cell* **21**, 245–256 (2011).
50. M. Liu, Z. Feng, H. Ke, Y. Liu, T. Sun, J. Dai, W. Cui, J. C. Pastor-Pareja, Tango1 spatially organizes ER exit sites to control ER export. *J. Cell Biol.* **216**, 1035–1049 (2017).
51. S. Ito, K. Nagata, Biology of Hsp47 (Serpin H1), a collagen-specific molecular chaperone. *Semin. Cell Dev. Biol.* **62**, 142–151 (2017).
52. L. Bassaganyas, S. J. Popa, M. Horlbeck, C. Puri, S. E. Stewart, F. Campelo, A. Ashok, C. M. Butnaru, N. Brouwers, K. Heydari, J. Ripoche, J. Weissman, D. C. Rubinsztein, R. Schekman, V. Malhotra, K. Moreau, J. Villeneuve, New factors for protein transport identified by a genome-wide CRISPRi screen in mammalian cells. *J. Cell Biol.* **218**, 3861–3879 (2019).
53. J. E. Galán, G. Waksman, Protein-Injection machines in bacteria. *Cell* **172**, 1306–1318 (2018).
54. F. G. Sauer, J. S. Pinkner, G. Waksman, S. J. Hultgren, Chaperone priming of pilus subunits facilitates a topological transition that drives fiber formation. *Cell* **111**, 543–551 (2002).
55. J. Nanchahal, B. Hinz, Strategies to overcome the hurdles to treat fibrosis, a major unmet clinical need. *Proc. Natl. Acad. Sci. U.S.A.* **113**, 7291–7293 (2016).
56. J. Varga, B. Pasche, Antitransforming growth factor-beta therapy in fibrosis: Recent progress and implications for systemic sclerosis. *Curr. Opin. Rheumatol.* **20**, 720–728 (2008).
57. C. Y. Ewald, J. N. Landis, J. Porter Abate, C. T. Murphy, T. K. Blackwell, Dauer-independent insulin/IGF-1-signalling implicates collagen remodelling in longevity. *Nature* **519**, 97–101 (2015).
58. S. Ricard-Blum, G. Baffet, N. Théret, Molecular and tissue alterations of collagens in fibrosis. *Matrix Biol.* **68–69**, 122–149 (2018).
59. S. Brenner, The genetics of *Caenorhabditis elegans*. *Genetics* **77**, 71–94 (1974).
60. R. S. Kamath, J. Ahringer, Genome-wide RNAi screening in *Caenorhabditis elegans*. *Methods* **30**, 313–321 (2003).
61. B. Lehner, J. Tischler, A. G. Fraser, RNAi screens in *Caenorhabditis elegans* in a 96-well liquid format and their application to the systematic identification of genetic interactions. *Nat. Protoc.* **1**, 1617–1620 (2006).
62. C. C. Mello, J. M. Kramer, D. Stinchcomb, V. Ambros, Efficient gene transfer in *C. elegans*: Extrachromosomal maintenance and integration of transforming sequences. *EMBO J.* **10**, 3959–3970 (1991).
63. A. B. Byrne, M. T. Weirauch, V. Wong, M. Koeva, S. J. Dixon, J. M. Stuart, P. J. Roy, A global analysis of genetic interactions in *Caenorhabditis elegans*. *J. Biol.* **6**, 8 (2007).

Acknowledgments: We thank the *Caenorhabditis* Genetics Center and the National BioResource Project in Japan for *C. elegans* strains. We thank K. Atabai, A. Hata, and M. Shoulders for the discussions; J. Pastor-Pareja for the transgenic *Drosophila* line; B. Canque for the TMEM131L plasmid reagents; and V. Malhotra, I. Raote, J. Villeneuve, and H. Zhang for communication of the research findings. **Funding:** This work was supported by the NIH grant R01GM117461, the Shurl and Kay Curci Foundation Faculty Scholarship from the Innovative Genomics Institute, the Pew Scholar Award, and the Packard Fellowship in Science and Engineering (to D.K.M.). **Author contributions:** All authors participated in the experimental design, execution, or data interpretation and analysis. Z.Z. and D.K.M. wrote the paper. **Competing interests:** The authors declare that they have no competing interests. **Data and materials availability:** All data needed to evaluate the conclusions in the paper are present in the paper and/or the Supplementary Materials. Additional data related to this paper may be requested from the authors.

Submitted 16 July 2019
Accepted 26 November 2019
Published 12 February 2020
10.1126/sciadv.aay7667

Citation: Z. Zhang, M. Bai, G. O. Barbosa, A. Chen, Y. Wei, S. Luo, X. Wang, B. Wang, T. Tsukui, H. Li, D. Sheppard, T. B. Kornberg, D. K. Ma, Broadly conserved roles of TMEM131 family proteins in intracellular collagen assembly and secretory cargo trafficking. *Sci. Adv.* **6**, eaay7667 (2020).

Science Advances

Broadly conserved roles of TMEM131 family proteins in intracellular collagen assembly and secretory cargo trafficking

Zhe Zhang, Meirong Bai, Guilherme Oliveira Barbosa, Andrew Chen, Yuehua Wei, Shuo Luo, Xin Wang, Bingying Wang, Tatsuya Tsukui, Hao Li, Dean Sheppard, Thomas B. Kornberg and Dengke K. Ma

Sci Adv **6** (7), eaay7667.
DOI: 10.1126/sciadv.aay7667